


Article

Modeling and Experimental Studies on Carbon Dioxide Absorption with Sodium Hydroxide Solution in a Rotating Zigzag Bed

Zhibang Liu ¹, Arash Esmaeili ¹, Hanxiao Zhang ¹, Dan Wang ^{2,3}, Yuan Lu ⁴ and Lei Shao ^{1,*} 

- ¹ Research Center of the Ministry of Education for High Gravity Engineering and Technology, Beijing University of Chemical Technology, Beijing 100029, China; 2019400002@mail.buct.edu.cn (Z.L.); ar.esmaeli@mail.buct.edu.cn (A.E.); 2018200070@mail.buct.edu.cn (H.Z.)
- ² State Key Laboratory of Petroleum Pollution Control, Beijing 102206, China; wang-dan@cnpc.com.cn
- ³ CNPC Research Institute of Safety and Environmental Technology, Beijing 102206, China
- ⁴ CenerTech Oilfield Chemical Co., Ltd., Tianjin 300450, China; luyuan2@cnooc.com.cn
- * Correspondence: shaol@mail.buct.edu.cn; Tel.: +86-10-6442-1706

Abstract: The enhancement of mass transfer is very important in CO₂ absorption, and a rotating zigzag bed (RZB) is a promising device to intensify the gas–liquid mass transfer efficiency. In this study, the mass transfer characteristics in an RZB in relation to the overall gas-phase volumetric mass-transfer coefficient (K_{Ga}) were investigated with a CO₂–NaOH system. A mathematical model was established to illustrate the mechanism of the gas–liquid mass transfer with irreversible pseudo-first-order reaction in the RZB. The effects of various operating conditions on K_{Ga} were examined. Experimental results show that a rise in the liquid flow rate, inlet gas flow rate, rotational speed, absorbent temperature, and absorbent concentration was conducive to the mass transfer between gas and liquid in the RZB. It was found that the rotational speed had the largest impact on K_{Ga} in the RZB. The K_{Ga} predicted by the model agreed well with that by the experiments, with deviations generally within 10%. Therefore, this model can be employed to depict the mass transfer process between gas and liquid in an RZB and provide guidance for the application of RZBs in CO₂ absorption.

Keywords: rotating zigzag bed; modeling; gas–liquid mass transfer; carbon dioxide; absorption



Citation: Liu, Z.; Esmaeili, A.; Zhang, H.; Wang, D.; Lu, Y.; Shao, L. Modeling and Experimental Studies on Carbon Dioxide Absorption with Sodium Hydroxide Solution in a Rotating Zigzag Bed. *Processes* **2022**, *10*, 614. <https://doi.org/10.3390/pr10030614>

Academic Editors: Elio Santacesaria, Riccardo Tesser and Vincenzo Russo

Received: 21 February 2022

Accepted: 17 March 2022

Published: 21 March 2022

Publisher's Note: MDPI stays neutral with regard to jurisdictional claims in published maps and institutional affiliations.



Copyright: © 2022 by the authors. Licensee MDPI, Basel, Switzerland. This article is an open access article distributed under the terms and conditions of the Creative Commons Attribution (CC BY) license (<https://creativecommons.org/licenses/by/4.0/>).

1. Introduction

The rotating zigzag bed (RZB) is an emerging high-gravity device with an innovative zigzag passage structure to enhance fluid turbulence and mass transfer [1,2]. Liquid disperses and coalesces repeatedly by colliding with the rotating and static baffles continuously in the zigzag passage, leading to a high surface renewal frequency of the liquid [3]. Correspondingly, a significant increase in the gas–liquid contact time and liquid holdup is achieved in the RZB, which is in favor of mass transfer [4]. Compared to the conventional rotating packed bed (RPB), the RZB also exhibits the advantages of no demand for the liquid distributor and static seal, easy realization of the intermediate feed, and configuration of the multi-stage rotor in one casing [5,6]. Therefore, RZBs have been applied to stripping [7], distillation [5], extraction [8], and gas–liquid reaction [9,10].

Li et al. [10] studied the mass transfer characteristics of CO₂ absorption into NaOH solution in an RZB and found that the efficiency of liquid-side mass transfer in the RZB was significantly superior to that in the conventional RPB. Other research has demonstrated that the effective interfacial area and the efficiency of gas-side mass transfer were on par with those in RPBs with stainless wire mesh packing. In consideration of the rotor structure with zigzag channel, pressure drop and power requirement in RZB are higher than those in RPB [1,11]. However, in terms of the study of Liu et al. [12] on the features of CO₂ absorption and mass transfer with diethylenetriamine-based absorbents in an RZB, the

RZB exhibited a better performance on CO₂ absorption and mass transfer with decreased device size and absorbent usage in comparison with an RPB, which could make up for the above disadvantages of RZB and reduce the operating cost. Moreover, a smaller volume of RZB with higher gas–liquid mass transfer efficiency makes it more suitable for application in confined spaces, such as vessels and offshore platforms, relative to conventional columns and RPBs [12], suggesting that the RZB is a promising apparatus for intensifying the gas–liquid contact processes.

The overall volumetric mass transfer coefficient is a crucial index to assess the mass transfer performance of a gas–liquid contact device. Extensive studies on the modelling of the overall volumetric mass transfer coefficient between gas and liquid in RPBs or other high-gravity devices have been conducted [13–17]. Additionally, the modelling of local mass transfer in RPBs has also been proposed [18,19]. However, there are only a few reports on the performance of mass transfer in the RZB, such as experimental investigations on the effective interfacial area and local mass transfer coefficient [10] and qualitative analysis of the mass transfer characteristics [2]. To the best of our knowledge, there is no report on the modelling of overall volumetric mass transfer coefficient in the RZB. Therefore, modelling the gas–liquid mass transfer behavior described by the overall volumetric mass transfer coefficient in the RZB can provide a theoretical basis for process intensification in the RZB.

Herein, based on fluid flow in different regions of the rotor in an RZB, a mechanism model has been proposed for the first time to describe the reactive mass transfer process in the CO₂–NaOH system and predict the mass transfer performance in the RZB. The effects of various operating conditions on the overall gas-phase volumetric mass-transfer coefficient ($K_G a$) were studied. The model was validated by the agreement of the predicted values with the experimental results.

2. Materials and Methods

2.1. Materials

Granulated sodium hydroxide (purity 98.0%) was provided by Shanghai Macklin Biochemical Co., Ltd., Shanghai, China. A carbon dioxide cylinder (purity 99.0%) was supplied by Beijing Shunanqite Gas Co., Ltd., Beijing, China. Deionized water was used through the experiments.

2.2. Experimental Apparatuses and Procedure

The RZB used in this work is schematically shown in Figure 1 [12], and the specifications of the RZB are given in Table 1 [12].

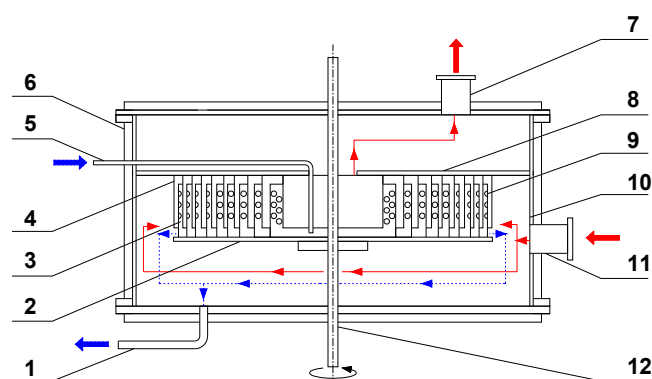


Figure 1. Structure of the rotating zigzag bed (RZB): (1) liquid outlet; (2) rotating disk; (3) rotating baffles; (4) static baffles; (5) liquid inlet; (6) insulation materials; (7) gas outlet; (8) static disk; (9) perforations; (10) shell; (11) gas inlet; (12) shaft. (Blue and red lines indicate liquid and gas streams, respectively).

Table 1. Specifications of the rotating zigzag bed (RZB).

Item	Value
Inner diameter of the rotor (cm)	5.7
Outer diameter of the rotor (cm)	18.3
Inner diameter of the shell (cm)	23.1
Diameter of the static baffles (cm)	5.7, 8.1, 9.9, 11.4, 12.7, 14.0, 15.2, 16.3, 17.3, 18.3
Diameter of the rotating baffles (cm)	7.2, 9.0, 10.7, 12.2, 13.5, 14.7, 15.8, 16.8, 17.8
Volume of the rotor (cm ³)	665
Axial depth of the rotor (cm)	2.8
Axial depth of the static baffles (cm)	2.5
Axial depth of the rotating baffles (cm)	2.4
Diameter of perforation in the rotating baffles (mm)	2.1

The rotor is the main component of the RZB. Static and rotating baffles are mounted alternately in the radial direction on the static and rotating disks, respectively, in the rotor. The upper section of the rotating baffles is perforated. The annular space between the static and rotating baffles forms the zigzag passage for fluid streams.

The shell of the RZB was covered with insulation materials to keep the reaction temperature in the RZB at a certain level, and an infrared thermometer (F-380, Shenzhen Flank Electronic Co., Ltd.) was employed to measure the temperature of the insulation materials.

The experimental setup is illustrated in Figure 2 [12]. The RZB was preheated by using a NaOH solution until a designated temperature was reached. A mixed gas stream containing air and CO₂ was then directed into the RZB via the gas inlet. When CO₂ concentration at the gas inlet reached 4%, the NaOH solution with a preset temperature was pumped into the RZB through the liquid inlet. The gas stream flowed inwards from the periphery of the rotor and made contact in a countercurrent with the liquid stream flowing outwards in the rotor to realize the absorption of CO₂ by the NaOH solution. Finally, the liquid and gas flows left the RZB via the liquid and gas outlets, respectively.

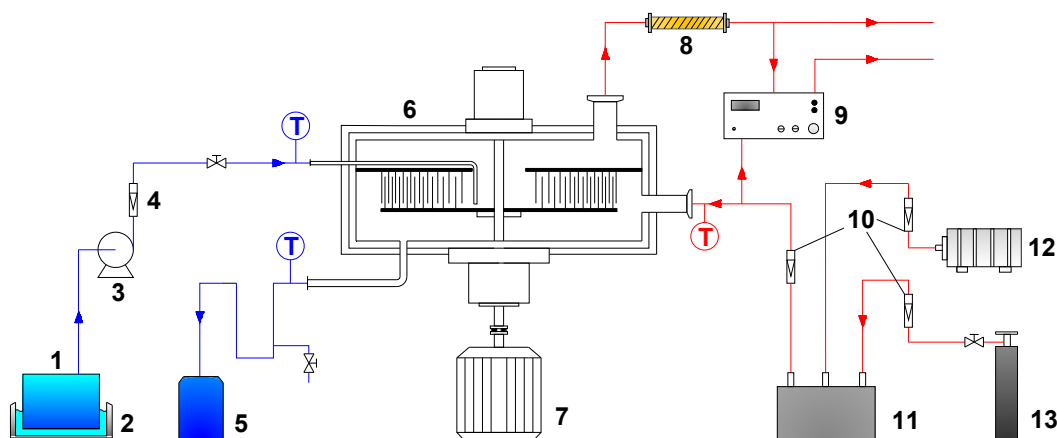


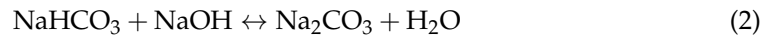
Figure 2. Experimental setup: (1) absorbent container; (2) thermostatic bath; (3) liquid pump; (4) liquid rotameter; (5) effluent tank; (6) RZB; (7) motor; (8) dryer; (9) CO₂ analyzer; (10) gas rotameter; (11) gas mixing tank; (12) air compressor; (13) CO₂ cylinder.

The experiments were performed at ambient pressure, and the experimental data were collected when a stable state of CO₂ absorption process was achieved. The concentration of CO₂ in gas streams entering and leaving the RZB was measured by an infrared CO₂ analyzer (GXH-3010F, Beijing Huayun Analytical Instrument Institution Co., Ltd., Beijing, China). All the experiments were repeated to validate the reproducibility of the results.

3. Theory

3.1. Reactions of CO₂ in Sodium Hydroxide Solution

When CO₂ is absorbed into the NaOH solution, the reactions between CO₂ with NaOH take place. These reactions can be expressed as follows [20]:



The rate of the above reactions can be calculated by the following second-order reaction rate equation [21]:

$$r_{\text{CO}_2} = k_2 C_{\text{NaOH}} C_{\text{CO}_2} \quad (3)$$

The reaction can be regarded as a pseudo-first-order one when in Equation (4) is satisfied [20,22].

$$\sqrt{1 + \frac{D_{\text{CO}_2} k_2 C_{\text{NaOH}}}{k_L^2}} - 1 \ll \frac{C_{\text{NaOH}}}{2C_0} \quad (4)$$

where D_{CO_2} is the diffusion coefficient of CO₂ in NaOH solution.

In this study, in Equation (4) held because the left-side of in Equation (4) was over 100 times smaller than the right-side. Therefore, the rate constant of the pseudo-first-order reaction can be written as:

$$k_{\text{app}} = k_2 C_{\text{NaOH}} \quad (5)$$

3.2. Gas and Liquid Flow in the RZB Rotor

Gas and liquid flows in the RZB rotor are presented in Figure 3. Gas flows inwards from the periphery to the center of the RZB rotor, and the gas velocity can be divided into tangential component (v_θ), radial component (v_r), and axial component (v_z) in this process. The ratio of the tangential velocity to the total velocity is 81.6% to 99.3% [23], suggesting that gas mainly moves in a spiral between the rotating and static baffles.

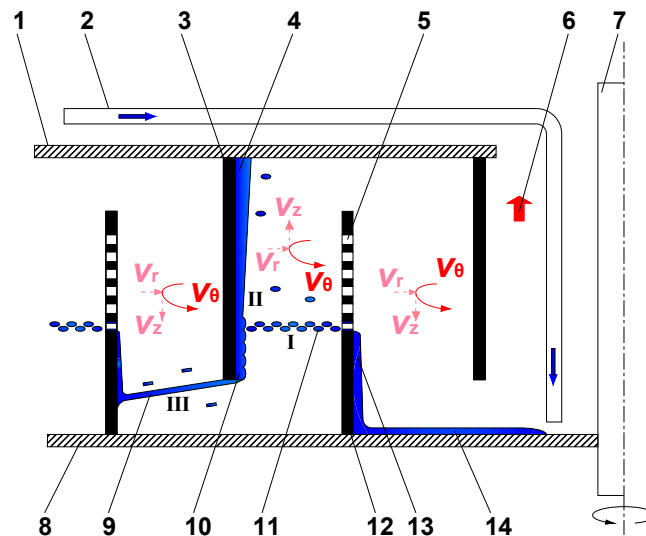


Figure 3. Side view of gas and liquid flow in RZB rotor: (1) static disk; (2) liquid inlet; (3) static baffle; (4) stagnant filmy liquid; (5) perforations; (6) gas stream; (7) shaft; (8) rotating disk; (9) flying filmy liquid; (10) turbulent filmy liquid; (11) flying fine droplets; (12) rotating baffle; (13) filmy liquid climbing up on the internal surface of rotating baffle; (14) filmy liquid on the rotating disk. (Red and blue symbols represent gas and liquid flows, respectively.).

The liquid flow moves outwards through the zigzag passage in the rotor. At the center of the rotating disk, liquid flows tangentially outwards under the action of centrifugal force

until it reaches the internal surface of the rotating baffle and then climbs up to the perforated area. The liquid is dispersed into fine droplets when passing through the perforations in the upper section of the rotating baffle and flies along a tangential direction to the static baffle. The fine droplets are captured by the static baffle to form a filmy liquid, which flows spirally downwards on the internal surface of the static baffle due to gravity and tangential movement of the liquid. The filmy liquid departs tangentially from the static baffle as a sheet and reaches the next rotating baffle without falling onto the rotating disk because the tangential liquid velocity is much larger than the axial liquid velocity caused by gravity. The liquid is then captured by the next rotating baffle and repeats the above process in the zigzag passage until leaving the RZB rotor [10].

In terms of the above gas and liquid flow characteristics in the RZB rotor, the gas–liquid contact area can be divided into three different zones, as shown in Figure 3, as zones I, II, and III, and all of them make contributions to the mass transfer [3]. In zone I, fine droplets contact with gas in a spiral movement in the space formed by the rotating and static baffles, contributing to the gas–liquid mass transfer. In zone II, mass transfer is scarcely attributed to contact between gas and the stagnant filmy liquid formed by droplets on the upper section of the static baffle, but mainly results from the surface renewal caused by droplets continually impinging on the turbulent filmy liquid on the lower section of the static baffle [2]. In zone III, the liquid exists as an intact sheet when there is no gas flow, but some fine droplets may result from rupture of the sheet when gas flows through the passage. The contact of the flying liquid and gas in zone III also contributes to mass transfer. Hence, the rotor of the RZB can be regarded as a series of wetted-wall columns with the centrifugal field [3].

It has been reported that mass transfer in zone II contributes most to the overall mass transfer because the continued horizontal impingement by liquid jets on the turbulent filmy liquid on the static baffles brings about a great surface renewal rate. Mass transfer in zones I and III is at least one order of magnitude less than that in zone II because the renewal time of the liquid surface in zones I and III is longer than that in zone II according to the penetration theory [2].

3.3. Model Development

According to the flow characteristics of gas and liquid in the RZB rotor, model assumptions for CO₂ absorption into the NaOH solution in the RZB were made as follows:

- (1) Velocity of droplets leaving the rotating baffle along the tangential direction in zone I was equal to the circumferential velocity of the rotating baffle [11].
- (2) Only the tangential velocity of gas phase in the RZB rotor was considered, and the radial and axial velocities of gas were ignored because the tangential velocity was the main component of the gas velocity [23].
- (3) It should be noted that the tangential gas velocity is smaller than the circumferential velocity of rotating baffles when the gas flow rate is low [23]. Because the gas flow rate was less than 1200 L/h in this study, the tangential gas velocity was much lower than the tangential liquid velocity in the space between the static baffle and rotating baffle. Thus, it was assumed that the effect of gas flow on the liquid form could be ignored in zone III, where the flying liquid remained in the form of an intact sheet [11]. Meanwhile, the liquid form in zones I and II was not affected by gas flow either.
- (4) Liquid existed as droplets in zone I and filmy liquid in zone II [10]. Hence, the overall gas–liquid effective interfacial area was the sum of the surface area of droplets in zone I, turbulent filmy liquid on the static baffle in zone II, and the flying intact liquid sheet in zone III [2,11].
- (5) Liquid left the rotating baffle only through the lowest circle of perforations in the rotating baffles because the perforations were closely spaced [24]. Droplets formed by every perforation had the same amount, lifetime, velocity, and diameter.

- (6) Liquid film is a thin surface layer in the filmy liquid. The liquid film in the turbulent filmy liquid in zone II was renewed by impingement of fine droplets from zone I, and the liquid film in the filmy liquid in every zone of the RZB had the same lifetime [2].
- (7) The reaction between CO_2 and NaOH was considered to be a pseudo-first-order reaction. The concentration of OH^- in the liquid film was assumed to be constant during the CO_2 absorption process, and thus k_{app} was regarded as a constant in the liquid element.

For the chemical absorption of CO_2 into NaOH solution, CO_2 is absorbed from the gas phase to the liquid phase via a gas–liquid interface. During this process, the gas–liquid mass transfer depends both on the liquid-phase and gas-phase mass transfer. Therefore, the gas–liquid effective interfacial area (a), liquid-side mass-transfer coefficient (k_L), and gas-side mass-transfer coefficient (k_G) should be considered for calculating $K_G a$.

The space in the rotor of the RZB was divided into certain annular regions for model development (Figure 4). Nine rotating baffles (1, 2, ..., i_a , $i_a + 1$, ..., 9) and ten static baffles (0', 1', ..., i_b , $i_b + 1$, ..., 9') were radially alternately arranged. Region i was the annular region between the rotating baffle i_a of radius $r_{a,i}$ and static baffle i_b of radius $r_{b,i}$, and region i' was the annular region between the static baffle i_b of radius $r_{b,i}$ and rotating baffle $i_a + 1$ of radius $r_{a,i+1}$. Mass transfer zones I and II were located in region i , while zone III was in region i' .

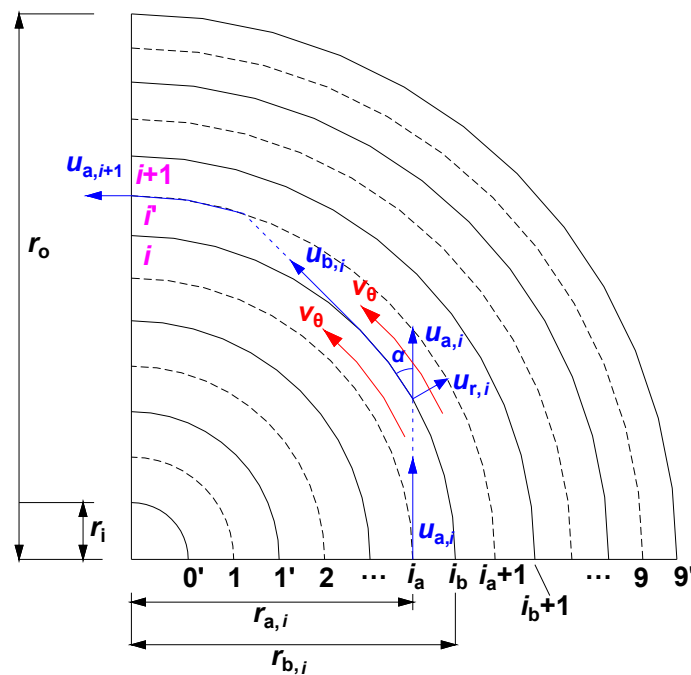


Figure 4. Top view of liquid and gas flows in the rotor of RZB.

In zone I of region i , droplets left the rotating baffle i_a of radius $r_{a,i}$ with a tangential velocity $u_{a,i}$ along the tangential direction to the static baffle i_b . The lifetime of droplets in zone I $t_{I,i}$ is written as:

$$t_{I,i} = \frac{\sqrt{r_{b,i}^2 - r_{a,i}^2}}{u_{a,i}} \quad (6)$$

$$u_{a,i} = \omega r_{a,i} \quad (7)$$

where ω represents the angular velocity of the RZB rotor.

The liquid holdup of droplets $\varepsilon_{L,i}$ in this area can be calculated by the following equation:

$$\varepsilon_{L,i} = \frac{Q_L t_{L,i}}{\pi(r_{b,i}^2 - r_{a,i}^2)z} = \frac{Q_L}{\pi\omega z r_{a,i} \sqrt{r_{b,i}^2 - r_{a,i}^2}} \quad (8)$$

where Q_L is the liquid volumetric flow rate in the RZB rotor and z is the axial depth of the rotor.

The correlation of the effective mass transfer area of droplets $A_{L,i}$ in zone I of region i is as follows [16]:

$$A_{L,i} = a_{L,i} \pi (r_{b,i}^2 - r_{a,i}^2) z = \frac{6\varepsilon_{L,i}}{d_i} \pi (r_{b,i}^2 - r_{a,i}^2) z \quad (9)$$

where d_i is the average diameter of droplets in zone I of region i .

In zone II of region i , the surface area of the turbulent filmy liquid is equal to the effective mass transfer area in this zone, which can be obtained by the following equation:

$$A_{II,i} = 2\pi r_{b,i} A_2 h_{II} \quad (10)$$

where A_2 is a turbulent coefficient used to correct the variation of surface area of the filmy liquid caused by the impingement of droplets (with a value of 2.19) [25] and h_{II} represents the axial length of the turbulent filmy liquid.

In zone III of region i' , the liquid remained in the form of an intact sheet between the static and rotating baffles according to assumption (4). The filmy liquid tangentially left the static baffle of radius $r_{b,i}$ with a tangential velocity of $u_{b,i}$, and thus the lifetime of the flying filmy liquid in zone III of region i' $t_{III,i'}$ is expressed as follows:

$$t_{III,i'} = \frac{\sqrt{r_{a,i+1}^2 - r_{b,i}^2}}{u_{b,i}} = \frac{\sqrt{r_{a,i+1}^2 - r_{b,i}^2}}{u_{a,i} \frac{r_{a,i}}{r_{b,i}}} \quad (11)$$

Thus, the surface area of the flying filmy liquid equals the gas–liquid effective mass transfer area in this zone:

$$A_{III,i'} = (2\pi r_{b,i} + 2\pi r_{a,i+1}) \sqrt{(r_{a,i+1} - r_{b,i})^2 + \left(u_{g,i} t_{III,i'} + \frac{1}{2} g t_{III,i'}^2\right)^2} \quad (12)$$

where $u_{g,i}$ is the axial component of the turbulent filmy liquid velocity in zone II.

Therefore, the gas–liquid effective interfacial area in the RZB rotor can be obtained as follows:

$$a = a_I + a_{II} + a_{III} = \frac{\sum_{i=1}^9 A_{L,i} + \sum_{i=1}^9 A_{II,i} + \sum_{i'=1}^8 A_{III,i'}}{\pi(r_0^2 - r_1^2)z} \quad (13)$$

The mass transfer in the liquid phase consists of that in the droplets and filmy liquid. Because the droplets were treated as rigid balls without inside circulation during the flight due to a small distance in zone I of region i [26], the following mass partial differential equation can be used to present the CO_2 diffusion process from gas bulk to droplets based on the pseudo-first-order irreversible chemical reaction:

$$\frac{\partial C_{\text{CO}_2}}{\partial t_{L,i}} = D_{\text{CO}_2} \frac{\partial^2 C_{\text{CO}_2}}{\partial R^2} + \frac{2D_{\text{CO}_2}}{R} \frac{\partial C_{\text{CO}_2}}{\partial R} - k_{\text{app}} (C_{\text{CO}_2} - C_{\text{CO}_2}^*) \quad (14)$$

$$\text{I.C. } t_{L,i} = 0, R \geq 0: C_{\text{CO}_2} = C_{\text{CO}_2}^*$$

$$\text{B.C. } R = 0, t_{L,i} \geq 0: C_{\text{CO}_2} = C_{\text{CO}_2}^*$$

$$R = \frac{d_i}{2}, t_{L,i} \geq 0: C_{\text{CO}_2} = C_0 \quad (15)$$

where $C_0 (=P_{\text{CO}_2,0}/H)$ and $C_{\text{CO}_2}^*$ are the molar concentration of CO_2 at the gas–liquid interface and the equilibrium molar concentration of CO_2 in the liquid bulk, respectively.

Letting $C_A = C_{\text{CO}_2} - C_{\text{CO}_2}^*$, the following expressions can be obtained:

$$\frac{\partial C_A}{\partial t_{1,i}} = D_{\text{CO}_2} \frac{\partial^2 C_A}{\partial R^2} + \frac{2D_{\text{CO}_2}}{R} \frac{\partial C_A}{\partial R} - k_{\text{app}} C_A \quad (16)$$

$$\text{I.C. } t_{1,i} = 0, R \geq 0: C_A = 0;$$

$$\text{B.C. } R = 0, t_{1,i} \geq 0: C_A = 0;$$

$$R = \frac{d_i}{2}, t_{1,i} \geq 0: C_A = C_0 - C_{\text{CO}_2}^*; \quad (17)$$

After Laplace transform, the following ordinary differential equation is derived:

$$\frac{d^2 u}{dR^2} + \frac{2}{R} \frac{du}{dR} - \frac{k_{\text{app}} + s}{D_{\text{CO}_2}} u = 0 \quad (18)$$

Letting $\beta = u \times R$, Equation (22) can be obtained by Equations (19)–(21).

$$\frac{d\beta}{dR} = \frac{du}{dR} R + u \quad (19)$$

$$\frac{d^2 \beta}{dR^2} = \frac{d^2 u}{dR^2} R + 2 \frac{du}{dR} \quad (20)$$

$$\frac{1}{R} \frac{d^2 \beta}{dR^2} = \frac{d^2 u}{dR^2} + \frac{2}{R} \frac{du}{dR} \quad (21)$$

$$\frac{d^2 \beta}{dR^2} = \frac{k_{\text{app}} + s}{D_{\text{CO}_2}} \beta \quad (22)$$

The general solution of β can be calculated by Equation (23):

$$\beta = u \times R = C_1 e^{-R \sqrt{\frac{k_{\text{app}} + s}{D_{\text{CO}_2}}}} + C_2 e^{R \sqrt{\frac{k_{\text{app}} + s}{D_{\text{CO}_2}}}} \quad (23)$$

Then, the following equation is obtained by Laplace inverse transform:

$$\begin{aligned} C_A = \frac{C_1}{2R} \exp \left(R \sqrt{\frac{k_{\text{app}}}{D_{\text{CO}_2}}} \right) \operatorname{erfc} \left(-\frac{R}{2\sqrt{D_{\text{CO}_2} t_{1,i}}} - \sqrt{k_{\text{app}} t_{1,i}} \right) \\ + \frac{C_1}{2R} \exp \left(-R \sqrt{\frac{k_{\text{app}}}{D_{\text{CO}_2}}} \right) \operatorname{erfc} \left(-\frac{R}{2\sqrt{D_{\text{CO}_2} t_{1,i}}} + \sqrt{k_{\text{app}} t_{1,i}} \right) \\ + \frac{C_2}{2R} \exp \left(-R \sqrt{\frac{k_{\text{app}}}{D_{\text{CO}_2}}} \right) \operatorname{erfc} \left(\frac{R}{2\sqrt{D_{\text{CO}_2} t_{1,i}}} - \sqrt{k_{\text{app}} t_{1,i}} \right) \\ + \frac{C_2}{2R} \exp \left(R \sqrt{\frac{k_{\text{app}}}{D_{\text{CO}_2}}} \right) \operatorname{erfc} \left(\frac{R}{2\sqrt{D_{\text{CO}_2} t_{1,i}}} + \sqrt{k_{\text{app}} t_{1,i}} \right) \end{aligned} \quad (24)$$

where $\operatorname{erfc}(x)$ is the excess error function.

To simplify Equation (24), B is defined as follows:

$$B = \exp \left(\frac{d_i}{2} \sqrt{\frac{k_{\text{app}}}{D_{\text{CO}_2}}} \right) \operatorname{erf} \left(\frac{\frac{d_i}{2}}{2\sqrt{D_{\text{CO}_2} t_{1,i}}} + \sqrt{k_{\text{app}} t_{1,i}} \right) + \exp \left(-\frac{d_i}{2} \sqrt{\frac{k_{\text{app}}}{D_{\text{CO}_2}}} \right) \operatorname{erf} \left(\frac{\frac{d_i}{2}}{2\sqrt{D_{\text{CO}_2} t_{1,i}}} - \sqrt{k_{\text{app}} t_{1,i}} \right) \quad (25)$$

where $\operatorname{erf}(x)$ is the error function.

Letting $C_1 = -C_2$ and substituting Equation (17) into Equation (24), C_1 and C_2 can be expressed as follows:

$$C_1 = \frac{C_0 - C_{\text{CO}_2}^*}{2B} d_i \quad (26)$$

$$C_2 = -C_1 = -\frac{C_0 - C_{\text{CO}_2}^*}{2B} d_i \quad (27)$$

Therefore, Equation (28) can be obtained by combining Equations (24), (26) and (27):

$$C_A = \frac{(C_0 - C_{\text{CO}_2}^*) d_i}{2RB} \exp\left(R\sqrt{\frac{k_{\text{app}}}{D_{\text{CO}_2}}}\right) \operatorname{erf}\left(\frac{R}{2\sqrt{D_{\text{CO}_2} t_{L,i}}} + \sqrt{k_{\text{app}} t_{L,i}}\right) + \frac{(C_0 - C_{\text{CO}_2}^*) d_i}{2RB} \exp\left(-R\sqrt{\frac{k_{\text{app}}}{D_{\text{CO}_2}}}\right) \operatorname{erf}\left(\frac{R}{2\sqrt{D_{\text{CO}_2} t_{L,i}}} - \sqrt{k_{\text{app}} t_{L,i}}\right) \quad (28)$$

In terms of Fick's first law, the rate equation describing mass transfer at the gas-liquid interface can be written as:

$$k_{L-I,i} (C_{\text{CO}_2} - C_{\text{CO}_2}^*) = D_{\text{CO}_2} \frac{\partial C_A}{\partial R} \Big|_{R=\frac{d_i}{2}} \quad (29)$$

It was assumed that CO_2 was completely consumed by chemical reaction of CO_2 and NaOH in the liquid bulk. Thus, $C_{\text{CO}_2}^*$ can be ignored, and $k_{L-I,i}$ in zone I is given by Equation (30):

$$k_{L-I,i} = \sqrt{k_{\text{app}} D_{\text{CO}_2}} - \frac{2D_{\text{CO}_2}}{d_i} \quad (30)$$

In regard to liquid film in the turbulent filmy liquid in zone II of region i , CO_2 diffusion into the liquid film with a pseudo-first-order reaction can be expressed as:

$$\frac{\partial C_{\text{CO}_2}}{\partial t_{\text{II},i}} = D_{\text{CO}_2} \frac{\partial^2 C_{\text{CO}_2}}{\partial x^2} - k_{\text{app}} (C_{\text{CO}_2} - C_{\text{CO}_2}^*) \quad (31)$$

$$I.C. \ t_{\text{II},i} = 0, \ x \geq 0: \ C_{\text{CO}_2} = C_{\text{CO}_2}^*;$$

$$B.C. \ x = 0, \ t_{\text{II},i} \geq 0: \ C_{\text{CO}_2} = C_0;$$

$$x = \delta (\rightarrow \infty), \ t_{\text{II},i} \geq 0: \ C_{\text{CO}_2} = C_{\text{CO}_2}^* \quad (32)$$

where δ is the average thickness of the liquid film in zone II and $t_{\text{II},i}$ is the lifetime of the liquid film, which is the average time consumed for renewing the liquid film once.

The following equation can be obtained from Equations (31) and (32):

$$\frac{\partial C_A}{\partial t_{\text{II},i}} = D_{\text{CO}_2} \frac{\partial^2 C_A}{\partial x^2} - k_{\text{app}} C_A \quad (33)$$

$$I.C. \ t_{\text{II},i} = 0, \ x \geq 0: \ C_A = 0;$$

$$B.C. \ x = 0, \ t_{\text{II},i} \geq 0: \ C_A = C_0 - C_{\text{CO}_2}^*;$$

$$x = \delta (\rightarrow \infty), \ t_{\text{II},i} \geq 0: \ C_A = 0; \quad (34)$$

By Laplace transform, the following equation is derived:

$$\frac{d^2 u}{dx^2} - \frac{k_{\text{app}} + s}{D_{\text{CO}_2}} u = 0 \quad (35)$$

$$B.C. \ x = 0, \ s \geq 0: \ u = \frac{C_0 - C_{\text{CO}_2}^*}{s};$$

$$x = \delta (\rightarrow \infty), \ s \geq 0: \ u = 0; \quad (36)$$

Substituting the boundary conditions in Equation (36) into Equation (35), the general solution of u can be obtained by Equation (37):

$$u = \frac{C_0 - C_{CO_2}^*}{s} \exp\left(-x\sqrt{\frac{k_{app} + s}{D_{CO_2}}}\right) \quad (37)$$

By the Laplace inverse transform, the relationship of the CO₂ concentration distribution, lifetime, and liquid film thickness can be described by the following equation:

$$C_A = \frac{(C_0 - C_{CO_2}^*)}{2} \exp\left(x\sqrt{\frac{k_{app}}{D_{CO_2}}}\right) \operatorname{erfc}\left(\frac{x}{2\sqrt{D_{CO_2}t_{II,i}}} + \sqrt{k_{app}t_{II,i}}\right) + \frac{(C_0 - C_{CO_2}^*)}{2} \exp\left(-x\sqrt{\frac{k_{app}}{D_{CO_2}}}\right) \operatorname{erfc}\left(\frac{x}{2\sqrt{D_{CO_2}t_{II,i}}} - \sqrt{k_{app}t_{II,i}}\right) \quad (38)$$

Hence, the mass transfer rate at the gas–liquid interface in zone II can be obtained based on Fick's first law.

$$R_{CO_2-II,i} = D_{CO_2} \frac{\partial C_A}{\partial x} \Big|_{x=0} = (C_0 - C_{CO_2}^*) \left(\sqrt{k_{app}D_{CO_2}} \operatorname{erf}\sqrt{k_{app}t_{II,i}} + \sqrt{\frac{D_{CO_2}}{\pi t_{II,i}}} \exp(-k_{app}t_{II,i}) \right) \quad (39)$$

According to assumptions (5) and (6), the renewal of the liquid film in zone II was caused by the impingement of droplets, which came from the lowest circle of the perforated area in the rotating baffle. It was assumed that the droplets formed by every perforation had the same amount, lifetime, velocity, and diameter. Therefore, the renewal frequency, S_i , defined as the number of droplets leaving the rotating baffles per unit time, in zone II of region i is expressed as:

$$S_i = \frac{36Q_L}{\pi n_{a,i} d_i^3} \quad (40)$$

where $n_{a,i}$ is the number of perforations in the rotating baffle i_a .

Then the lifetime of the liquid film in the turbulent film liquid can be calculated by Equation (41) [18]:

$$t_{II,i} = \frac{1}{S_i} \quad (41)$$

It was assumed that $t_{II,i}$ caused by every droplet was the same. Thus, Equation (42) can be used to express the Higbie distribution function of the lifetime of the liquid film [16]:

$$\psi(t_{II,i}) = \frac{1}{t_{II,i}} \quad (42)$$

Hence, the relationship between the liquid-side mass-transfer coefficient in zone II ($k_{L-II,i}$) and the mass transfer rate of liquid film at the gas–liquid interface can be written as:

$$\int_0^{t_{II,i}} R_{CO_2-II,i} \psi(t_{II,i}) dt = k_{L-II,i} (C_0 - C_{CO_2}^*) \quad (43)$$

Based on the same assumption for droplets, $C_{CO_2}^*$ can be ignored. Therefore, $k_{L-II,i}$ related to k_{app} , D_{CO_2} , and $t_{II,i}$ can be deduced as follows:

$$k_{L-II,i} = \frac{\sqrt{k_{app}D_{CO_2}}}{t_{II,i}} \left[t_{II,i} \operatorname{erf}\left(\sqrt{k_{app}t_{II,i}}\right) + \sqrt{\frac{t_{II,i}}{\pi k_{app}}} \exp(-k_{app}t_{II,i}) + \frac{1}{2k_{app}} \operatorname{erf}\left(\sqrt{k_{app}t_{II,i}}\right) \right] \quad (44)$$

As for the liquid film in the flying film liquid in zone III of region i' , the model development process of $k_{L-III,i'}$ was the same as that of $k_{L-II,i}$, and thus the expression of

$k_{L-III,i'}$ was similar to that of $k_{L-II,i}$, except for the lifetime of the liquid film in the flying filmy liquid, which was calculated by Equation (11).

Hence, $k_L a$ in the RZB rotor is written as follows:

$$k_L a = k_{L-I} a_I + k_{L-II} a_{II} + k_{L-III} a_{III} = \frac{\sum_{i=1}^9 k_{L-I,i} A_{I,i} + \sum_{i=1}^9 k_{L-II,i} A_{II,i} + \sum_{i'=1}^8 k_{L-III,i'} A_{III,i'}}{\pi(r_0^2 - r_1^2)z} \quad (45)$$

To date, there is no available expression to calculate k_G in the RZB rotor. Thus, a surface renewal model reported by Guo et al. [27] was employed to calculate k_G in the RZB rotor as follows:

$$k_G = \sqrt{D_G k_s v_\theta^2} \quad (46)$$

where D_G is the diffusion coefficient of CO_2 in gas phase, k_s is the proportionality coefficient, and v_θ is the average tangential gas velocity in the RZB rotor.

The $K_G a$ of the RZB can be calculated by [15]:

$$\frac{1}{K_G a} = \frac{1}{k_G a} + \frac{H}{k_L a} \quad (47)$$

The experimental $K_G a$ can be determined by Equation (48), which was obtained in the previous study on CO_2 absorption [12]:

$$K_G a = \frac{G'}{\pi P z (r_0^2 - r_1^2)} \left[\ln \frac{y_{\text{CO}_2-\text{in}} (1 - y_{\text{CO}_2-\text{out}})}{y_{\text{CO}_2-\text{out}} (1 - y_{\text{CO}_2-\text{in}})} + \left(\frac{y_{\text{CO}_2-\text{in}}}{1 - y_{\text{CO}_2-\text{in}}} - \frac{y_{\text{CO}_2-\text{out}}}{1 - y_{\text{CO}_2-\text{out}}} \right) \right] \quad (48)$$

where G' is the inlet gas flow rate of inert gas (without reaction or dissolution), P is the total pressure, and $y_{\text{CO}_2-\text{in}}$ and $y_{\text{CO}_2-\text{out}}$ denote the molar fraction of CO_2 in the inlet and outlet gas streams, respectively.

By substituting the experimental $K_G a$ from Equation (48) and the calculated $k_L a$ and a from Equations (45) and (13), respectively, into Equation (47), k_G can be obtained. Consequently, k_s can be obtained, which is necessary for the establishment of the mass transfer model. Thus, the calculated k_G , $k_L a$, and $K_G a$ for the RZB were obtained from this mass transfer model.

The density and viscosity values were obtained from reference [28], while the surface tension value was from reference [29]. The equilibrium, kinetics, and transport parameters used for modeling are tabulated in Table 2.

Table 2. Parameters for model development.

Parameter	Expression
H [30]	$\log \frac{H}{H_W} = \sum hI$
H_W [30]	$H_W = 101.3 * (23.9 + 0.757(T/^\circ\text{C} - 18))$
D_{CO_2} [31]	$D_{\text{CO}_2} \mu_L = D_W \mu_W$
D_W [31]	$\log D_W = -8.1764 + \frac{712.5}{T} - \frac{2.591 \times 10^5}{T^2}$
D_G [32]	$D_G = 2.189 \times 10^{-5} - 0.393 \times 10^{-5} [\text{OH}^-]$
k_2 [31]	$\log \frac{k_2}{k_{\text{OH}^-}^\infty} = 0.2211 - 0.016I^2$
$k_{\text{OH}^-}^\infty$ [31]	$\log k_{\text{OH}^-}^\infty = 11.895 - \frac{2382}{T}$
d_i [27]	$d_i = 0.7284 \left(\frac{\sigma}{\omega^2 r_{a,i} \rho_L} \right)^{0.5}$
v_θ [23]	$\frac{v_\theta}{v_{\text{in}}} = 101.9987 Re_G^{-0.7004} \left(\frac{r_m}{r_a} \right)^{-1.6356} \left(\frac{\omega^2 r_a}{g} \right)^{-0.4384}$
$u_{g,i}$ [25]	$u_{g,i} = \left(\frac{\rho_L g Q_L^2}{3\pi^2 \mu_L (2r_{b,i})^2} \right)^{\frac{1}{3}}$

4. Results and Discussion

4.1. Model Validation

The RZB had an average value for k_s of $6.17 \times 10^{-8} \text{ kmol}^2 \text{ s/kPa}^2 \text{ m}^8$ under the experimental conditions. By using k_L , k_G , and a obtained from the above model and the average value of k_s , the calculated $K_G a$ of the RZB was obtained according to Equation (47). The comparison of k_L , k_G , and a between this work and reference [10] can be found in Table S1 in the Supplementary Materials file.

Figure 5 is the diagonal diagram of the predicted and experimental values of $K_G a$. It is shown that this model provided good predictions on $K_G a$ of CO_2 absorption in the RZB, with deviations generally less than 10% in comparison with the experimental results. Additionally, in the Figures shown in Sections 4.2–4.6, the curves for the predicted values were consistent with those for the experimental results. In addition, the values of individual and overall mass transfer parameters have been presented in Table S2 in the Supplementary Materials file.

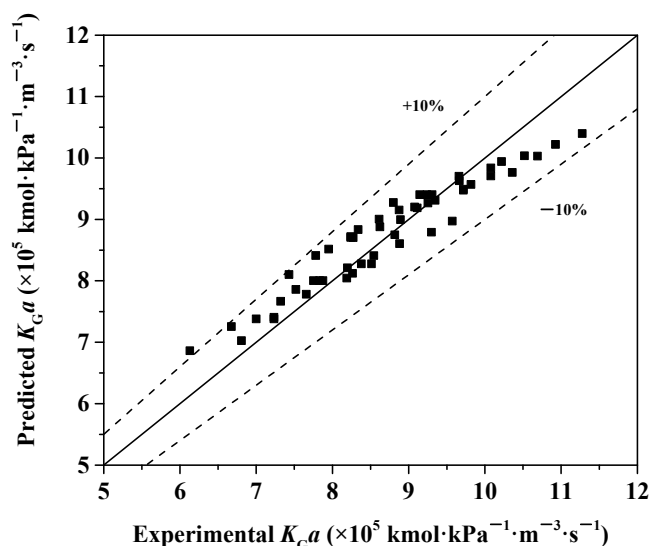


Figure 5. Diagonal diagram of experimental and predicted $K_G a$.

4.2. Effect of Liquid Flow Rate

Figure 6 presents the effect of the liquid flow rate on $K_G a$ in the RZB. It can be seen that $K_G a$ in NaOH solution obviously increased, with a rise in the liquid flow rate from 25 to 40 L/h.

With a rising liquid flow rate, more fine droplets from the rotating baffles are produced. The falling velocity of the filmy liquid on the static baffles also increases in terms of the expression of $u_{g,i}$ in Table 2, causing an increasing area of the flying liquid sheet between the static and rotating baffles according to Equation (12). These factors enhance the liquid holdup in the RZB, thereby causing a rising gas–liquid contact area based on Equation (8). Meanwhile, with the increase of the liquid flow rate, the circumferential distribution of droplets in zone I is improved [10], and more droplets continually impinge on the filmy liquid on the lower section of the static baffles, leading to an enhancement of liquid turbulence and a higher surface renewal rate of liquid film in the turbulent filmy liquid in zone II, as suggested by Equation (40), which are conducive to the liquid-side mass transfer. Therefore, a higher liquid flow rate brought about a larger $K_G a$ in this study because a and k_L contributed notably to $K_G a$ for CO_2 absorption into NaOH solution.

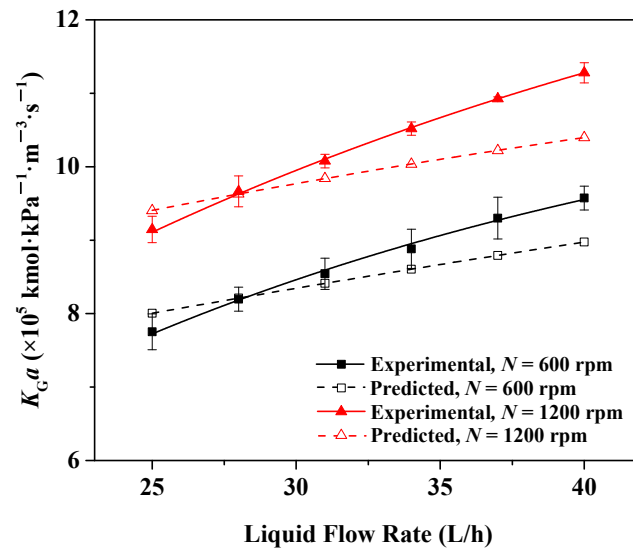


Figure 6. Effect of liquid flow rate on K_{Ga} in the RZB ($G = 1000$ L/h, $T = 298.15$ K, $T_{\text{gas}} = 298.15$ K, $y_{\text{CO}_2\text{-in}} = 4\%$, $C_{\text{NaOH}} = 0.15$ kmol/m³).

4.3. Effect of Inlet Gas Flow Rate

The influence of the inlet gas flow rate on K_{Ga} in the RZB is given in Figure 7, which shows that K_{Ga} in the NaOH solution rose from 6.13×10^{-5} to 8.26×10^{-5} kmol/kPa m³ s and from 6.67×10^{-5} to 9.65×10^{-5} kmol/kPa m³ s, with the inlet gas flow rate increasing from 200 to 1200 L/h at the rotational speed of 600 rpm and 1200 rpm, respectively.

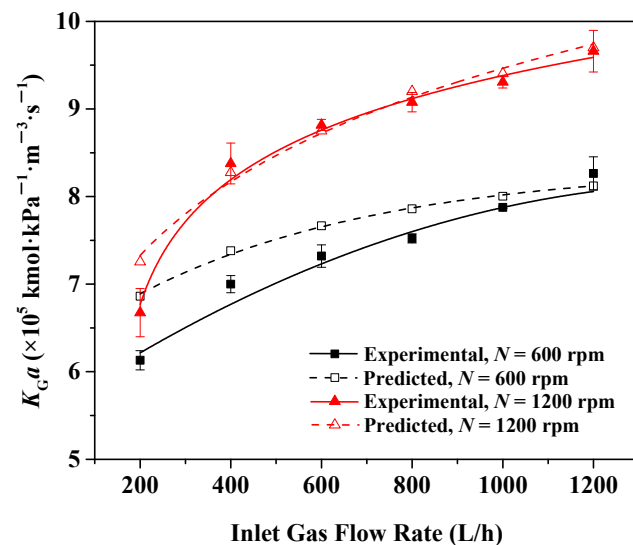


Figure 7. Effect of inlet gas flow rate on K_{Ga} in the RZB ($L = 25$ L/h, $T = 298.15$ K, $T_{\text{gas}} = 298.15$ K, $y_{\text{CO}_2\text{-in}} = 4\%$, $C_{\text{NaOH}} = 0.15$ kmol/m³).

Because K_{Ga} in the NaOH solution is affected by k_{Ga} , a rising inlet gas flow rate in the RZB increases the tangential gas velocity in the annular space between the rotating and static baffles, which leads to the increase of gas turbulence and a decrease of gas film thickness [16]. Therefore, the mass transfer resistance in the gas side reduces and consequently k_{Ga} increases, thereby enhancing K_{Ga} in the RZB. Hence, an increasing inlet gas flow rate brought about a rise in K_{Ga} in the experimental range.

4.4. Effect of Rotational Speed

The variation of K_{Ga} with the rotational speed is shown in Figure 8. K_{Ga} augmented with a rise in the rotational speed from 400 to 1200 rpm.

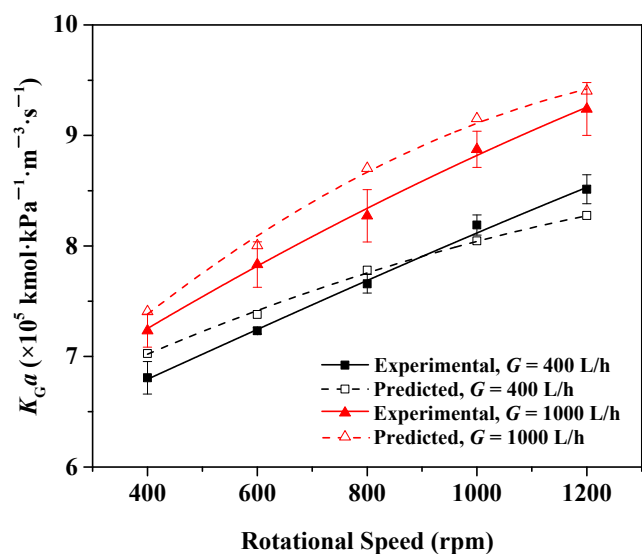


Figure 8. Effect of rotational speed on $K_G a$ in the RZB ($L = 25$ L/h, $T = 298.15$ K, $T_{\text{gas}} = 298.15$ K, $y_{\text{CO}_2\text{-in}} = 4\%$, $C_{\text{NaOH}} = 0.15$ kmol/m³).

When the rotational speed rises, a larger centrifugal force is created by the rotating baffles, leading to an enhanced liquid turbulence and higher tangential velocity of droplets departing from the rotating baffles according to Equation (7), which reduces the size of droplets in the space between the rotating and static baffles based on the expression of droplet diameter in Table 2. Therefore, a in zone I increase.

At the same time, rising rotational speed causes an increase in the number of droplets impinging on the turbulent film liquid as a result of the reduction in droplet size and a larger circumferential velocity of the turbulent film liquid in zone II, which is equal to the tangential velocity of the flying liquid sheet leaving the static baffles in zone III [11], resulting in a rise in the surface renewal frequency of the liquid film in the turbulent film liquid on the static baffles in terms of Equation (40) and a decrease in the lifetime of the flying liquid sheet in zone III according to Equation (11). The former factor brought about an increase in k_{L-II} in zone II, and the latter factor was conducive to k_{L-III} in zone III according to Equation (44).

The above analysis indicates that a higher rotational speed led to higher a and k_L , which markedly enhanced $K_G a$ of the CO₂-NaOH system in the RZB.

4.5. Effect of Absorbent Temperature

The effect of the absorbent temperature on $K_G a$ is presented in Figure 9. The figure indicates that a higher temperature of NaOH solution is favorable for $K_G a$, which increased from 7.95×10^{-5} to 8.80×10^{-5} kmol/kPa m³ s and from 9.35×10^{-5} to 1.02×10^{-4} kmol/kPa m³ s with an increase in temperature from 293.15 to 313.15 K at the liquid flow rate of 25 L/h and 35 L/h, respectively.

In accordance with the Arrhenius equation for the reaction rate constant in Table 2, a higher temperature of NaOH solution increases the second-order rate constant k_2 , thereby leading to a larger pseudo-first-order reaction rate constant k_{app} , which is favorable for the liquid-side mass transfer performance. Moreover, the resistance in liquid-side mass transfer reduces and the diffusion of CO₂ in the liquid phase is improved with increasing temperature [12]. These factors promoted mass transfer and caused a higher k_L , thereby leading to an increasing $K_G a$.

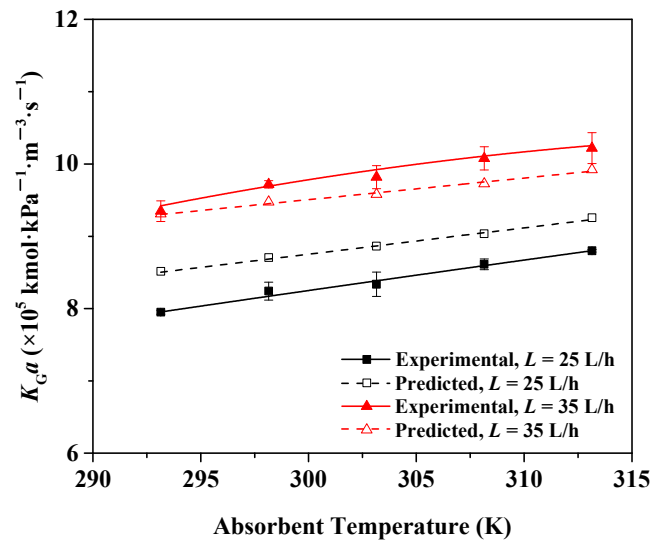


Figure 9. Effect of absorbent temperature on K_{Ga} in the RZB ($G = 1000$ L/h, $N = 800$ rpm, $T_{gas} = 298.15$ K, $y_{CO_2-in} = 4\%$, $C_{NaOH} = 0.15$ kmol/m³).

4.6. Effect of Absorbent Concentration

Figure 10 illustrates the effect of NaOH absorbent concentration on K_{Ga} in the RZB. It is noted that K_{Ga} increased from 7.43×10^{-5} to 9.25×10^{-5} kmol/kPa m³ s with an increase in the absorbent concentration from 0.1 to 0.2 mol/L at the liquid flow rate of 25 L/h, while K_{Ga} increased from 8.62×10^{-5} to 1.07×10^{-4} kmol/kPa m³ s as the absorbent concentration rose from 0.1 to 0.2 kmol/m³ at the liquid flow rate of 35 L/h.

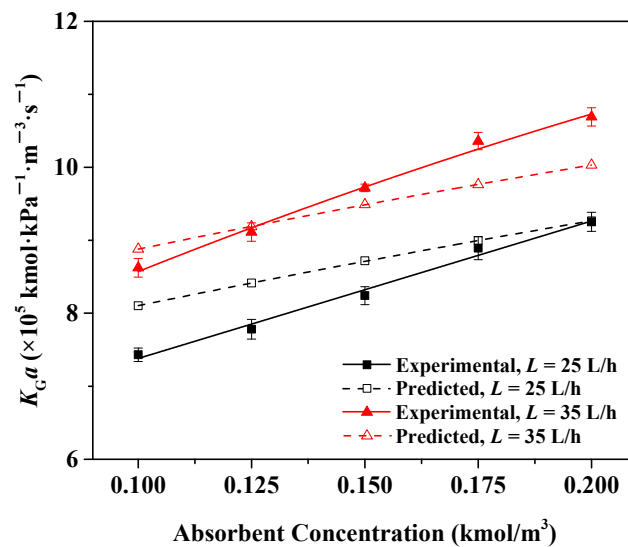


Figure 10. Effect of absorbent concentration on K_{Ga} in the RZB ($G = 1000$ L/h, $N = 800$ rpm, $T = 298.15$ K, $T_{gas} = 298.15$ K, $y_{CO_2-in} = 4\%$).

When the concentration of NaOH solution increases, the second-order reaction rate constant between CO₂ and the absorbent rises according to the expression of k_2 shown in Table 2. Meanwhile, a higher k_2 and C_{NaOH} can concurrently enhance the pseudo-first-order reaction rate constant k_{app} , causing a higher k_L in every mass transfer zone of the RZB. Hence, K_{Ga} increased with an increasing NaOH concentration.

4.7. Comparison between Spray Column and RZB

Table 3 reveals comparative results of mass transfer efficiency between a spray column and the RZB. It was found that the experimental K_{Ga} in the spray column was less than

that in the RZB on the basis of a similar gas–liquid volume ratio. Additionally, the RZB possessed a greater mass transfer efficiency accompanied by a much lower NaOH solution concentration compared to the spray column, suggesting that an obvious enhancement of mass transfer in CO₂ absorption can be realized by the RZB.

Table 3. Comparison between spray column and RZB.

	Javed et al. [33]	This Work
Reactor	Spray column	RZB
Mass transfer zone volume (cm ³)	9813	665
Liquid flow rate (L/h)	120–300	25–40
Gas–liquid volume ratio	32–42	25–40
Rotational speed (rpm)	/	400–1200
Absorbent	1.25 kmol/m ³ NaOH	0.10–0.20 kmol/m ³ NaOH
Inlet CO ₂ concentration (%)	2.5	4
Absorbent temperature (K)	ca. 298 K	298 K
K_{Ga} (10 ⁵ × kmol/kPa m ³ s)	2.65–4.56	6.81–11.28

Considering an enhanced dispersion and coalescence of the liquid phase in the annular regions between the static and rotating baffles, a shorter lifetime of the liquid element in the RZB is gained compared to the spray column, and the intensification of mass transfer is thus expected in the RZB, conducting to the CO₂ absorption process.

5. Conclusions

In this study, by obtaining the analytical expressions of the gas–liquid effective interfacial area, liquid-side and gas-side mass-transfer coefficients in an RZB, a mathematic model of CO₂ absorption into NaOH solution with irreversible pseudo-first-order reaction in the RZB was established to quantitatively describe the gas–liquid mass transfer process and predict K_{Ga} .

The K_{Ga} calculated by the model was consistent with the experimental data under different operating conditions. The calculated K_{Ga} exhibited deviations generally less than 10% in comparison with the experimental data, which demonstrated the excellent predictability of this model for CO₂ absorption in an RZB. Meanwhile, the influences of various operating conditions on K_{Ga} in the RZB were predicted reasonably by this model. Experimental results indicate that higher liquid flow rate, inlet gas flow rate, rotational speed, absorbent temperature, and absorbent concentration favored gas–liquid mass transfer in the RZB. It was found that the rotational speed had the largest impact on K_{Ga} in the RZB. This study provides the theoretical basis for potential application of RZBs in CO₂ absorption.

Supplementary Materials: The following supporting information can be downloaded at: <https://www.mdpi.com/article/10.3390/pr10030614/s1>, Table S1: Comparison of mass transfer performance between RZB in this work and that in Reference 10; Table S2: Values of individual and overall mass transfer factors in RZB.

Author Contributions: Conceptualization, L.S.; methodology, Z.L.; validation, A.E.; formal analysis, H.Z.; investigation, D.W.; resources, Y.L.; data curation, Z.L.; writing—original draft preparation, Z.L.; writing—review and editing, Z.L.; supervision, L.S.; project administration, L.S.; funding acquisition, L.S. All authors have read and agreed to the published version of the manuscript.

Funding: This research was funded by the National Natural Science Foundation of China, grant number 22178021.

Institutional Review Board Statement: Not applicable.

Informed Consent Statement: Not applicable.

Data Availability Statement: Not applicable.

Acknowledgments: The authors gratefully acknowledge financial support from the National Natural Science Foundation of China (No. 22178021).

Conflicts of Interest: The authors declare no conflict of interest.

Nomenclature

a	gas–liquid effective interfacial area, m^2/m^3
$a_{\text{I}}, a_{\text{II}}, a_{\text{III}}$	gas–liquid effective interfacial area in zone I, II, and III, respectively, m^2/m^3
$a_{\text{I},i}$	gas–liquid effective interfacial area in zone I of region i , m^2/m^3
$A_{\text{I},i}, A_{\text{II},i}$	effective mass transfer area in zone I and II of region i , respectively, m^2
$A_{\text{III},i'}$	effective mass transfer area in zone III of region i' , m^2
A_2	turbulent coefficient
C_A	difference between actual and equilibrium CO_2 concentration in liquid phase, kmol/m^3 , $C_A = C_{\text{CO}_2} - C_{\text{CO}_2}^*$
C_{CO_2}	concentration of CO_2 in liquid phase, kmol/m^3
$C_{\text{CO}_2}^*$	equilibrium concentration of CO_2 in liquid bulk, kmol/m^3
C_0	concentration of CO_2 at gas–liquid interface, kmol/m^3
C_{NaOH}	concentration of NaOH solution, kmol/m^3
d_i	average droplet diameter in zone I of region i , m
D_{CO_2}	diffusion coefficient of CO_2 in NaOH solution, m^2/s
D_G	diffusion coefficient of CO_2 in gas phase, m^2/s
D_W	diffusion coefficient of CO_2 in water, m^2/s
g	acceleration of gravity, m/s^2
G	inlet gas flow rate, L/h
G'	inlet flow rate of inert gas (without reaction and dissolution), kmol/s
h	constant related to h_+ , h_- , h_g , m^3/kmol
h_+, h_-, h_g	constant of cation, anion, and gas, respectively, m^3/kmol
h_{II}	axial length of turbulent filmy liquid, m
H	Henry's constant of NaOH solution, $\text{kPa m}^3/\text{kmol}$
H_W	Henry's constant of water, $\text{kPa m}^3/\text{kmol}$
I	ionic strength, kmol/m^3
k_2	second-order reaction rate constant, $\text{m}^3/\text{kmol s}$
k_{app}	pseudo-first-order rate constant, 1/s
k_G	gas-side mass-transfer coefficient, $\text{kmol}/\text{kPa m}^2 \text{ s}$
$K_G a$	overall gas-phase volumetric mass-transfer coefficient, $\text{kmol}/\text{kPa m}^3 \text{ s}$
k_L	liquid-side mass-transfer coefficient, m/s
$k_{\text{L-I}}, k_{\text{L-II}}, k_{\text{L-III}}$	liquid-side mass-transfer coefficient in zone I, II, and III, respectively, m/s
$k_{\text{L-I},i}, k_{\text{L-II},i}$	liquid-side mass-transfer coefficient in zone I and II of region i , respectively, m/s
$k_{\text{L-III},i'}$	liquid-side mass-transfer coefficient in zone III of region i' , m/s
$k_{\text{L}a}$	liquid-side volumetric mass-transfer coefficient, 1/s
$k_{\text{OH}^-}^\infty$	reaction rate constant in infinitely dilute NaOH solution, $\text{m}^3/\text{kmol s}$
k_s	proportionality coefficient, $\text{kmol}^2 \text{ s}/\text{kPa}^2 \text{ m}^8$
L	liquid flow rate, L/h
$n_{a,i}$	number of perforations in rotating baffle i_a
P	gas phase pressure, kPa
$P_{\text{CO}_2,0}$	partial pressure of CO_2 in gas phase at gas–liquid interface, kPa
Q_G	gas volumetric flow rate, m^3/s
Q_L	liquid volumetric flow rate, m^3/s
$r_{a,i}$	radius of rotating baffle i_a , m
$r_{b,i}$	radius of static baffle i_b , m
r_h	hydraulic radius of annular region between rotating and static baffles, m
r_i	inner radius of rotor, m
r_o	outer radius of rotor, m
r_m	radius of logarithmic mean, m
r_{CO_2}	reaction rate of CO_2 with NaOH solution, $\text{kmol}/\text{m}^3 \text{ s}$
R	radial coordinate of a droplet, m

$R_{\text{CO}_2\text{-II},i}$	mass transfer rate of liquid film at the gas–liquid interface in zone II of region i , mol/m ² s
Re_G	gas Reynolds number, $Re_G = \frac{4r_h v_G \rho_G}{\mu_G}$
s	complex variable
S_i	renewal frequency of liquid film in zone II of region i , 1/s
$t_{\text{I},i}$	lifetime of droplets in zone I of region i , s
$t_{\text{II},i}$	lifetime of liquid film in turbulent filmy liquid in zone II of region i , s
$t_{\text{III},i}$	lifetime of liquid film in flying filmy liquid in zone III of region i' , s
T	absorbent temperature, K
T_{gas}	gas temperature at gas inlet of RZB, K
$u_{a,i}$	tangential velocity of droplets leaving rotating baffle i_a , m/s
$u_{b,i}$	tangential velocity of flying filmy liquid leaving static baffle i_b , m/s
$u_{r,i}$	radial component of $u_{a,i}$, m/s
$u_{g,i}$	axial component of turbulent filmy liquid velocity on static baffle i_b , m/s
v_G	gas velocity in annular region between rotating and static baffles, m/s
v_θ	average tangential component of gas velocity, m/s
v_r	radial component of gas velocity, m/s
v_z	axial component of gas velocity, m/s
v_{in}	gas velocity at gas inlet of RZB, m/s
x	liquid film thickness of filmy liquid from gas–liquid interface, m
$y_{\text{CO}_2\text{-in}}$	molar fraction of CO ₂ in gas inlet of RZB, %
$y_{\text{CO}_2\text{-out}}$	molar fraction of CO ₂ in gas outlet of RZB, %
z	axial depth of rotor, m
α	angle between $u_{a,i}$ and tangent to static baffle i_b , °
ω	angular velocity, rad/s
$\varepsilon_{\text{I},i}$	liquid holdup of droplets in zone I of region i
δ	average thickness of liquid film in zone II, m
ρ_G	density of gas phase, kg/m ³
ρ_L	density of NaOH solution, kg/m ³
μ_G	viscosity of gas phase, pa s
μ_L	viscosity of NaOH solution, pa s
μ_W	viscosity of water, pa s
σ	surface tension of NaOH solution, N/m

References

- Li, Y.; Liu, P.; Wang, G.; Ji, J. Enhanced mass transfer and reduced pressure drop in a compound rotating zigzag bed. *Sep. Purif. Technol.* **2020**, *250*, 117188. [[CrossRef](#)]
- Wang, G.; Zhou, Z.; Li, Y.; Ji, J. Qualitative relationships between structure and performance of rotating zigzag bed in distillation. *Chem. Eng. Process.-Process Intensif.* **2019**, *135*, 141–147. [[CrossRef](#)]
- Wang, G.; Xu, Z.; Ji, J. Progress on hige distillation—Introduction to a new device and its industrial applications. *Chem. Eng. Res. Des.* **2011**, *89*, 1434–1442. [[CrossRef](#)]
- Wang, G.; Xu, Z.; Yu, Y.; Ji, J. Performance of a rotating zigzag bed—A new Hige. *Chem. Eng. Process.-Process Intensif.* **2008**, *47*, 2131–2139. [[CrossRef](#)]
- Wang, G.; Xu, O.; Xu, Z.; Ji, J. New Hige-rotating zigzag bed and its mass transfer performance. *Ind. Eng. Chem. Res.* **2008**, *47*, 8840–8846. [[CrossRef](#)]
- Li, Y.; Li, X.; Wang, Y.; Chen, Y.; Ji, J.; Yu, Y.; Xu, Z. Distillation in a counterflow concentric-ring rotating bed. *Ind. Eng. Chem. Res.* **2014**, *53*, 4821–4837. [[CrossRef](#)]
- Wang, Z.; Yang, T.; Liu, Z.; Wang, S.; Gao, Y.; Wu, M. Mass transfer in a rotating packed bed: A critical review. *Chem. Eng. Process.-Process Intensif.* **2019**, *139*, 78–94. [[CrossRef](#)]
- Karmakar, S.; Bhowal, A.; Das, P. A comparative study of liquid-liquid extraction in different rotating bed contactors. *Chem. Eng. Process.-Process Intensif.* **2018**, *132*, 187–193. [[CrossRef](#)]
- Liang, Z.; Wei, T.; Xie, J.; Li, H.; Liu, H. Direct conversion of terminal alkenes to aldehydes via ozonolysis reaction in rotating zigzag bed. *J. Iran. Chem. Soc.* **2020**, *17*, 2379–2384. [[CrossRef](#)]
- Li, Y.; Lu, Y.; Liu, X.; Wang, G.; Nie, Y.; Ji, J. Mass-transfer characteristics in a rotating zigzag bed as a Hige device. *Sep. Purif. Technol.* **2017**, *186*, 156–165. [[CrossRef](#)]
- Li, Y.; Yu, Y.; Xu, Z.; Li, X.; Liu, X.; Ji, J. Rotating zigzag bed as trayed Hige and its power consumption. *Asia-Pac. J. Chem. Eng.* **2013**, *8*, 494–506. [[CrossRef](#)]

12. Liu, Z.; Esmaili, A.; Zhang, H.; Xiao, H.; Yun, J.; Shao, L. Carbon dioxide absorption with aqueous amine solutions promoted by piperazine and 1-methylpiperazine in a rotating zigzag bed. *Fuel* **2021**, *302*, 121165. [[CrossRef](#)]
13. Zhang, L.; Wang, J.; Xiang, Y.; Zeng, X.; Chen, J. Absorption of carbon dioxide with ionic liquid in a rotating packed bed contactor: Mass transfer study. *Ind. Eng. Chem. Res.* **2011**, *50*, 6957–6964. [[CrossRef](#)]
14. Yi, F.; Zou, H.; Chu, G.; Shao, L.; Chen, J. Modeling and experimental studies on absorption of CO₂ by benfield solution in rotating packed bed. *Chem. Eng. J.* **2009**, *145*, 377–384. [[CrossRef](#)]
15. Sun, B.; Wang, X.; Chen, J.; Chu, G.; Chen, J.; Shao, L. Simultaneous absorption of CO₂ and NH₃ into water in a rotating packed bed. *Ind. Eng. Chem. Res.* **2009**, *48*, 11175–11180. [[CrossRef](#)]
16. Wang, D.; Liu, T.; Ma, L.; Wang, F.; Shao, L. Modeling and experimental studies on ozone absorption into phenolic solution in a rotating packed bed. *Ind. Eng. Chem. Res.* **2019**, *58*, 7052–7062. [[CrossRef](#)]
17. Zhao, Z.; Zhang, X.; Li, G.; Chu, G.; Sun, B.; Zou, H.; Arowo, M.; Shao, L. Mass transfer characteristics in a rotor-stator reactor. *Chem. Eng. Technol.* **2017**, *40*, 1078–1083. [[CrossRef](#)]
18. Qian, Z.; Xu, L.; Cao, H.; Guo, K. Modeling study on absorption of CO₂ by aqueous solutions of n-methyldiethanolamine in rotating packed bed. *Ind. Eng. Chem. Res.* **2009**, *48*, 9261–9267. [[CrossRef](#)]
19. Zhang, L.; Wang, J.; Liu, Z.; Lu, Y.; Chu, G.; Wang, W.; Chen, J. Efficient capture of carbon dioxide with novel mass-transfer intensification device using ionic liquids. *AIChE J.* **2013**, *59*, 2957–2965. [[CrossRef](#)]
20. Luo, Y.; Chu, G.; Zou, H.; Wang, F.; Xiang, Y.; Shao, L.; Chen, J. Mass transfer studies in a rotating packed bed with novel rotors: Chemisorption of CO₂. *Ind. Eng. Chem. Res.* **2012**, *51*, 9164–9172. [[CrossRef](#)]
21. Tsai, C.; Chen, Y. Effective interfacial area and liquid-side mass transfer coefficients in a rotating bed equipped with baffles. *Sep. Purif. Technol.* **2015**, *144*, 139–145. [[CrossRef](#)]
22. Li, Y.; Si, J.; Arowo, M.; Liu, Z.; Sun, B.; Song, Y.; Chu, G.; Shao, L. Experimental investigation of effective gas-liquid specific interfacial area in a rotor-stator reactor. *Chem. Eng. Process.-Process Intensif.* **2020**, *148*, 107801. [[CrossRef](#)]
23. Wang, H.; Li, Y.; Ji, J. Experimental study on gas flow field in a rotating zigzag bed. *Chin. J. Process Eng.* **2010**, *10*, 56–59. (In Chinese)
24. Li, Y.; Lu, Y.; Wang, G.; Nie, Y.; Ying, H.; Ji, J.; Liu, X. Liquid entrainment and flooding in a rotating zigzag bed. *Ind. Eng. Chem. Res.* **2015**, *54*, 2554–2563. [[CrossRef](#)]
25. Lu, Y.; Li, Y.; Yu, Y.; Liu, X.; Ji, J. Study on liquid hold-up of rotating zigzag bed. *Chin. J. Process Eng.* **2014**, *14*, 568–572. (In Chinese)
26. Cao, Z. Investigation into the Absorption in a Cyclone Absorber of Spraying Liquid from Side Wall. Ph.D. Thesis, South Yangtze University, Wuxi, China, 2008. (In Chinese).
27. Guo, F.; Zheng, C.; Guo, K.; Feng, Y.; Gardner, N. Hydrodynamics and mass transfer in cross-flow rotating packed bed. *Chem. Eng. Sci.* **1997**, *52*, 3853–3859. [[CrossRef](#)]
28. Liu, G.; Ma, L.; Xing, Z. *Handbook of Chemical Property Chart*; Chemical Industry Press: Beijing, China, 2002; pp. 47–163. (In Chinese)
29. Dutcher, C.; Wexler, A.; Clegg, S.L. Surface tensions of inorganic multicomponent aqueous electrolyte solutions and melts. *J. Phys. Chem. A* **2010**, *114*, 12216–12230. [[CrossRef](#)] [[PubMed](#)]
30. Sheng, M.; Xie, C.; Sun, B.; Luo, Y.; Zhang, L.; Chu, G.; Zou, H.; Chen, J. Effective mass transfer area measurement using a CO₂-NaOH system: Impact of different sources of kinetics models and physical properties. *Ind. Eng. Chem. Res.* **2019**, *58*, 11082–11092. [[CrossRef](#)]
31. Pohorecki, R.; Moniuk, W. Kinetics of reaction between carbon dioxide and hydroxyl ions in aqueous electrolyte solutions. *Chem. Eng. Sci.* **1988**, *43*, 1677–1684. [[CrossRef](#)]
32. Rajan, S.; Kumar, M.; Ansari, M.J.; Rao, D.; Kaistha, N. Limiting gas liquid flows and mass transfer in a novel rotating packed bed (HiGee). *Ind. Eng. Chem. Res.* **2011**, *50*, 986–997. [[CrossRef](#)]
33. Javed, K.; Mahmud, T.; Purba, E. The CO₂ capture performance of a high-intensity vortex spray scrubber. *Chem. Eng. J.* **2010**, *162*, 448–456. [[CrossRef](#)]